A precise determination of the electroweak mixing angle from semileptonic neutrino scattering

CHARM Collaboration

J.V. Allaby, U. Amaldi, G. Barbiellini, M. Baubillier[1], F. Bergsma, A. Capone, W. Flegel, F. Grancagnolo[2], L. Lanceri[3], M. Metcalf, C. Nieuwenhuis, R. Pain[4], J. Panman, R. Plunckett[5], K. Winter
CERN, CH-1211 Geneva 23, Switzerland

I. Abt, J. Aspiazu, A. Bungener, F.W. Büsser, P.D. Gall, T. Hebbeker, F. Niebergall, P. Schütt, P. Stähelin
II. Institut für Experimentalphysik[6], Universität Hamburg, D-2000 Hamburg, Federal Republic of Germany

P. Gorbunov, E. Grigoriev, V. Khovansky, A. Rosanov
Institute for Theoretical and Experimental Physics, SU-117259 Moscow, USSR

A. Baroncelli[7], L. Barone[8], B. Borgia[8], C. Bosio[7], M. Diemoz[8], C. Dionisi[8], U. Dore[8], F. Ferroni[8], E. Longo[8], P.F. Loverre[8], L. Luminari[8], P. Monacelli[8], S. Morganti[8], F. de Notaristefani[8], C. Santoni[9], L. Tortora[7], V. Valente[10]
Istituto Nazionale di Fisica Nucleare, I-00100 Rome, Italy

Abstract. The cross-section ratio of neutral-current and charged-current semileptonic interactions of muon-neutrinos on isoscalar nuclei has been measured with the result: $R^v = 0.3093 \pm 0.0031$ for hadronic energy larger than 4 GeV. From this ratio we determined the electroweak mixing angle $\sin^2 \theta_W = 0.236 + 0.012(m_c - 1.5) \pm 0.005(\text{exp.}) \pm 0.003(\text{theor.})$, where m_c is the charm-quark mass in GeV/c². Comparison with direct measurements of m_W and m_Z determines the radiative shift of the intermediate boson mass $\Delta r = 0.077 \pm 0.025(\text{exp.}) \pm 0.038(\text{syst.})$, in agreement with the prediction. Assuming the validity of the electroweak standard theory we determined $\varrho = 0.990 - 0.013(m_c - 1.5) \pm 0.009(\text{exp.}) \pm 0.003(\text{theor.})$.

I Introduction

The Standard Model of the electroweak gauge theory is successful in describing a large amount of experimental data [1]. Parity violation in atomic transitions [2], the asymmetry in the scattering of polarized electrons on deuterium [3], the neutral-current induced elastic scattering of muon-neutrinos on electrons [4, 5] and on protons [6], deep inelastic semileptonic neutrino scattering by the neutral weak current [7, 8], and the direct observation of the weak bosons [9, 10] are all consistent with universal strength of the forces associated with the $SU(2)$ and $U(1)$ symmetry groups of the standard model.

The fundamental quantities of the Standard Model, g and g', and the masses of the weak bosons, m_W and m_Z, are related to the angle θ_W that describes the mixing of the two local symmetries through the relations

$$\tan \theta_w = g'/g, \tag{1}$$

$$\sin^2 \theta_w = 1 - m_W^2/m_Z^2. \tag{2}$$

Table 1. Values of $\sin^2 \theta_W$ obtained from various processes and the values after electroweak radiative corrections have been applied

Experiment	$\sin^2 \theta_W^{unc}$	Condition	$\sin^2 \theta_W^{corr}$
Parity violation in Cs atoms [2]	0.221 ± 0.027		0.228 ± 0.027
eD scattering asymmetry [3]	0.224 ± 0.020	$\varrho = 1$	0.218 ± 0.020
$\nu_\mu(\bar{\nu}_\mu)e$ scattering [4]	0.215 ± 0.034	independent of ϱ	0.215 ± 0.034
$\nu_\mu(\bar{\nu}_\mu)e$ scattering [5]	0.209 ± 0.032	independent of ϱ	0.209 ± 0.032
$\nu_\mu(\bar{\nu}_\mu)p$ scattering [6]	0.220 ± 0.016	$M_A = 1.05$ GeV	0.220 ± 0.016
$\nu_\mu N$ deep inel. scattering [7]	0.232 ± 0.014	$\varrho = 1$	0.223 ± 0.014
$\nu_\mu N$ deep inel. scattering [8]	0.239 ± 0.012	$\varrho = 1$	0.226 ± 0.012
m_W and m_Z [9]	0.219 ± 0.015	$\varrho = 1$	0.214 ± 0.016
m_W and m_Z [10]	0.215 ± 0.008	$\varrho = 1$	0.232 ± 0.008

The value of this mixing parameter is not predicted by the model. It can be determined experimentally from measurements of the processes mediated by the neutral weak current. The values thus determined from various types of experiment are shifted by electroweak radiative corrections which have to be taken into account to perform a precise test of the theory. Because of the gauge nature of the interaction these radiative corrections can be calculated to all orders. Table 1 summarizes measured and corrected values of $\sin^2 \theta_W$ up to 1985. The agreement of the values corrected for electroweak radiative effects is excellent, whereas the measured values differ from each other.

A more advanced test of the theory, at the level of the radiative corrections of order α, can be performed by a precise determination of $\sin^2 \theta_W$ from semileptonic neutrino scattering and the direct measurements of m_W and m_Z. The Fermi interaction, mediated by the weak bosons, leads to a relation between the fine-structure constant α, the Fermi coupling constant G_F, the boson masses, and the weak mixing parameter $\sin^2 \theta_W$

$$m_W^2 = m_Z^2 \cos^2 \theta_W = \pi \alpha / \sqrt{2} G_F \sin^2 \theta_W. \tag{3}$$

Using $1/\alpha = 137.035963(15)$, as measured by the Josephson effect, and $G_F^\mu = 1.16637(2) \times 10^{-5}$ GeV^{-2} as determined from the muon lifetime, leads in lowest order to the relations:

$$\sin^2 \theta_W^{unc} = (37.281 \text{ GeV}/m_W)^2, \tag{4a}$$

$$\sin^2 2\theta_W^{unc} = (74.562 \text{ GeV}/m_Z)^2. \tag{4b}$$

Because of the definition of $\sin^2 \theta_W$ in (2) this relation must be radiatively corrected by using values of α and G_F at the mass of m_W. The change of the value of $G_F(m_W^2)$ is negligible, whereas α is changed to $\alpha(m_W) = \alpha(0)/(1 - \Delta r)$ with

$$\Delta r = 0.0713 \pm 0.0013, \tag{5}$$

assuming $m_{Higgs} = 100$ GeV and a top quark mass of $m_t = 45$ GeV [1, 11]. The predicted corresponding radiative shift of the W mass is about 3 GeV. The radiative correction can be experimentally determined from the measurements of m_W and m_Z and of $\sin^2 \theta_W$ through the relation

$$\Delta r = 1 - (\pi \alpha / m_W^2 \sqrt{2} G_F \sin^2 \theta_W) \tag{6}$$

and the corresponding relation involving m_Z. A comparison with the calculated radiative shift thus tests the predictive power of the Standard Model at the level of first-order radiative corrections in the same way as the predictive power of QED has been probed on the Lamb shift and on $(g-2)$ of the muon and the electron. The electroweak radiative shift is approximately 50 times larger than $(g-2)$ of the muon, owing to the larger masses of the weak bosons involved.

We report here on a precise determination of $\sin^2 \theta_W$ from semileptonic neutrino scattering* which allows this test to be performed at a sensitive level. The result puts constraints on new physics which might be appended to the Standard Model, on the mass of the top quark and of a hypothetical fourth generation charged lepton as well as on the mass of additional neutral gauge bosons. Furthermore, this measurement now provides an accurate value of $\sin^2 \theta_W$ which can be used to rule out, or at least constrain, Grand Unified Theories which predict it.

2 Determination of $\sin^2 \theta_W$ from semileptonic deep inelastic ν_μ scattering

Several methods can be used to determine a value of $\sin^2 \theta_W$ from semileptonic neutrino scattering. We have used a method recently proposed by Llewellyn Smith [12]. The coupling of the neutral weak current to fermions of charge q and the third component of weak isospin I_3 is according to the Standard Model:

$$g_L = 2(I_3 - q \sin^2 \theta_W), \tag{7a}$$

$$g_R = -2q \sin^2 \theta_W. \tag{7b}$$

---

* See also J.V. Allaby et al. (CHARM Collaboration): Phys. Lett. 177B (1986) 446

For the constituent u and d valence quarks of nucleons we thus expect

$$g_L^u = 1 - \tfrac{4}{3}\sin^2\theta_w, \qquad g_L^d = -1 + \tfrac{2}{3}\sin^2\theta_w, \qquad (8\,a)$$

$$g_R^u = -\tfrac{4}{3}\sin^2\theta_w, \qquad g_R^d = \tfrac{2}{3}\sin^2\theta_w. \qquad (8\,b)$$

Llewellyn Smith has shown that for isoscalar target nuclei the contribution of u, $\bar{u}$, and d, $\bar{d}$ quarks to the cross-sections of deep inelastic scattering of neutrinos by the neutral weak current (NC) and the charged weak current (CC) are related to $\sin^2\theta_w$ by the relation

$$d^2\sigma_{\mathrm{NC}}^{\nu(\bar{\nu})}/dx\,dy = (\tfrac{1}{2} - \sin^2\theta_w + \tfrac{5}{9}\sin^4\theta_w)\,d^2\sigma_{\mathrm{CC}}^{\nu(\bar{\nu})}/dx\,dy$$
$$+ \tfrac{5}{9}\sin^4\theta_w\,d^2\sigma_{\mathrm{CC}}^{\bar{\nu}(\nu)}/dx\,dy. \qquad (9)$$

Its validity depends on weak isospin symmetry. Integrating (9) over x and y, one obtains a relation containing only ratios of cross-sections,

$$R^\nu = \sigma_{\mathrm{NC}}^\nu/\sigma_{\mathrm{CC}}^\nu = \tfrac{1}{2} - \sin^2\theta_W + \tfrac{5}{9}\sin^4\theta_W(1+r), \qquad (10)$$

where $r = \sigma_{\mathrm{CC}}^{\bar{\nu}}/\sigma_{\mathrm{CC}}^\nu$.

A precise measurement of R^ν can be performed without the need to monitor precisely the incident neutrino flux. Events induced by neutrinos have to be classified as NC or CC events by the detection of a muon. One must, therefore, aim at a high efficiency of muon detection in designing a precise experiment. The track length of muons increases linearly with the mean neutrino energy and, hence, with parent (pion and kaon) beam momentum, whereas the length of hadron showers which may obscure the muon track increases only logarithmically with the beam momentum. Thus, a high-momentum parent beam is required. For a 160 GeV beam momentum, which was chosen as an optimum for the event statistics and the muon detection efficiency, more than 96% of the muons originating in CC reactions can be recognized; the losses can be calculated precisely, allowing a total experimental error of $\Delta R/R = \pm 0.01$ to be reached. A measurement of the ratio r of CC cross-sections for antineutrino and neutrino deep inelastic scattering is required to determine the correction term, $\tfrac{5}{9}r\sin^4\theta_W$, which accounts for NC scattering on right-handed quarks. The experimental precision required for r is reduced by the coefficient $\tfrac{5}{9}\sin^4\theta_W \approx 0.035$; hence a measurement error of $\Delta r/r = \pm 0.04$, because of the relative antineutrino and neutrino flux monitoring required, is sufficient to achieve a total experimental error of $\Delta\sin^2\theta_W = \pm 0.005$ at which we were aiming.

Equation (10) holds for deep inelastic scattering of neutrinos; processes which are not sensitive to the weak charge of the quarks, namely quasi-elastic scattering and coherent pion production, have to be rejected. This would be best achieved according to studies of deep inelastic scattering [13] by selecting events with a momentum transfer $Q^2 > 4\ \mathrm{GeV}^2$. In NC interactions a direct measurement of Q^2 is not possible, because the outgoing neutrinos are undetectable. However, for these near elastic processes there is a close relation between Q^2 and the hadron energy E_h. A selection of events with $E_h > 4$ GeV is an equivalent way of rejecting events which are not due to deep inelastic neutrino scattering.

Some processes contributing to deep inelastic scattering do break the isospin symmetry required for the validity of (10). These are mainly due to the asymmetry of the strange-quark sea and the charm-quark sea, owing to their different mass values, and to quark mixing. These asymmetries, amounting to $\Delta R^\nu/R^\nu \approx 2\%$, have to be corrected for by using the quark model to determine $\sin^2\theta_W$. The remaining uncertainties due to our present limited knowledge of the quark structure of nucleons have been estimated to contribute $\Delta\sin^2\theta_W = \pm 0.005$, the largest uncertainty being in the choice of the charm-quark mass which is required to describe the threshold of charm production in CC interactions. However, these uncertainties are expected to be reduced once better data are available to describe the quark structure of the nucleon.

The experimental set-up, consisting of the neutrino beam and the neutrino detector, and the data taking, trigger, and calibration procedure are described in Sect. 3. In Sect. 4 the analysis of the data, the determination of background, the classification of events, and the corrections applied to these classes are described. The results obtained after quark-model and radiative corrections have been applied, and their comparison with the results on m_W and m_Z obtained at the CERN $p\bar{p}$ collider, are described in Sect. 5. Their impact on physics is discussed in Sect. 6.

3 Experimental set-up

3.1 The narrow-band neutrino beam

The data were obtained in 1984 during a high-statistics exposure of the CHARM detector in the narrow-band neutrino beam at the CERN 450 GeV Super Proton Synchrotron (SPS). Neutrinos are produced in the decay of charge- and momentum-selected pions and kaons. Particles of positive or of negative charge produce a pure neutrino or antineutrino beam with a well-known energy spectrum. A small background, predominantly of low energy, the so-called wide-band (WB) background, is due to decays of particles which do not pass the charge and momentum selection of the beam line.

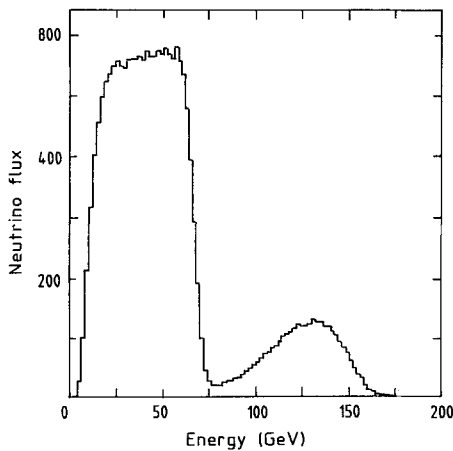A 160 GeV narrow band beam (NBB), developed

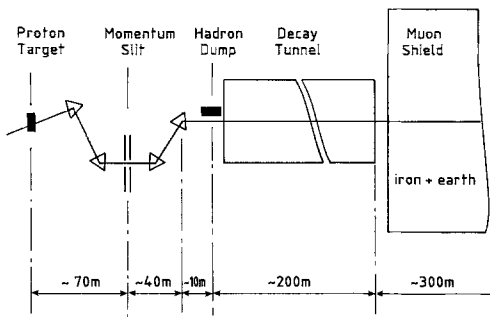**Fig. 1.** Energy spectrum of neutrino flux

Fig. 2. Schematic of the narrow-band-beam line

by Grant and Maugain [14] as a high-flux version of the CERN NBB optics, was used. The event rate per incident proton has been increased by about 50% by increasing the effective momentum bite of the beam with respect to the previous version of the NBB. The beam characteristics satisfy the conditions for a precision measurement of R^ν, namely [15]:

    i) A high average neutrino energy, needed for efficient muon recognition in the CHARM detector;

    ii) low background contributions, measurable with high accuracy;

    iii) the possibility of measuring the relative $\bar{\nu}/\nu$ flux normalization accurately;

    iv) calculable neutrino energy spectrum;

    v) high event rate.

The corresponding neutrino energy spectrum in the fiducial volume of the detector for accepted events is shown in Fig. 1. The contributions of pion and kaon decays are distinctly separated.

The elements of the beam line are shown schematically in Fig. 2. The beam travels in vacuum and is nearly parallel on entering the 300 m long decay tunnel. The vacuum is only interrupted at the place of a Cherenkov counter.

The components of the beam can be separated into four regions:

    i) The target region, where secondary hadrons are produced by a 450 GeV proton beam incident on a 3 cm diameter carbon target.

    ii) The secondary hadron beam line of about 120 m length, where hadrons are selected by sign and momentum and focused towards the decay region. The beam line was tuned to a central momentum of 160 GeV/c, with a momentum bite of $\pm 9\%$ (r.m.s.); the central momentum is known to about 3%. At the end of the beam line the angular divergence is ± 0.40 mrad in the horizontal plane and ± 0.48 mrad in the vertical plane.

    iii) About 8 m behind the last quadrupole magnet, hadrons enter a 292 m long decay tunnel, which was evacuated to a pressure of 0.15 Torr. The entrance window of the decay region is made of a 0.2 mm thick titanium membrane to minimize interactions of hadrons.

    iv) At the end of the decay tunnel all surviving hadrons are absorbed in the first few metres of a 185 m long iron shield. Muons are ranged out by a combination of the iron shield and a 220 m long earth shielding following it.

To avoid any losses of particles due to wrong steering of the beam, the onset of such bad conditions was detected by monitors surrounding the vacuum pipe. Various intensity monitors for both primary and secondary particles were placed along the beam line. The intensity of the ejected proton beam was measured by a beam-current transformer and the beam position on the 3 cm diameter carbon target was carefully monitored using a secondary emission chamber mounted ahead of the target. Another secondary emission chamber, downstream from the target, monitored the secondaries produced. Two identical beam-current transformers placed just in front of the entrance of the decay tunnel, after the last quadrupole lens, were used to measure the intensity of the secondary beam. The relative amounts of pions and kaons in the beam were determined experimentally using a helium-filled differential Cherenkov counter.

The beam could be closed by an iron dump just in front of the decay tunnel. Data were taken in this condition to determine experimentally the neutrino and antineutrino fluxes from decays ahead of the dump, the so-called WB background. To avoid background created by proton interactions in vacuum windows downstream from the dump which cannot be calculated well, the dump was placed inside an area which was part of the decay tunnel vacuum. The procedure used to correct for the WB background is described in Sect. 4.

The flux of muons originating from pion and kaon

Table 2. Exposures and dead-times

	ν	ν-dump	$\bar{\nu}$	$\bar{\nu}$-dump	GATE2
p.o.t. for data collection (10^{16})	338.0	113.2	97.8	49.0	–
p.o.t. selected (10^{16})	326.9	92.3	90.2	47.0	–
Dead-times (%):					
– unweighted	10.0	6.7	8.4	8.0	6.0
– flux weighted	16.5	10.7	14.0	14.9	–
– double events	3.0	1.1	1.2	0.4	0.1
Average dead-time (%)	19.0	11.8	15.0	15.3	6.1
p.o.t. corrected for dead-time (10^{16})	264.7	81.4	76.7	39.8	–
Integrated gate-time corrected for dead-time (s)	177.7	53.1	53.1	24.1	806.0
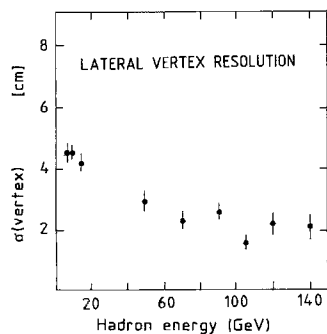
Fig. 3. Hadron shower vertex resolution

decays was measured by a system of solid-state detectors inserted into narrow gaps within the iron shield. They were also used to monitor the beam position and profile.

Pulse trains from scintillation counters located in the gaps of the iron shield were folded with the busy signals of the neutrino detector to determine the loss of neutrino events due to dead-time.

3.2 The CHARM detector

The CHARM neutrino detector is composed of a fine-grain calorimeter surrounded by a magnetized iron frame and of a muon spectrometer. The calorimeter has a sampling step corresponding to one radiation length or 0.22 pion absorption lengths, with scintillators, proportional drift tubes, and streamer tubes, as detecting elements. It is described in detail elsewhere [16].

The response of the calorimeter was calibrated in electron and pion beams in the range from 0.5 to 140 GeV/c [17]. The energy of hadron showers is measured by the scintillators with a resolution of

$$\sigma(E)/E = 0.487/\sqrt{(E/\text{GeV})} + 0.0127.$$

The lateral vertex position of hadron showers is determined by combining the measurements of all detection elements. The resolution is given in Fig. 3; it

reaches a precision of better than 3 cm above 50 GeV [17]. The muon momentum is measured by magnetic deflection; the resolution is $\sigma(p)/p \approx 15\%$ at low energies and increases to 20% at 150 GeV/c.

For this experiment the fiducial volume extended over 55 target plates, leaving five plates at the beginning of the detector to reject incoming tracks and 18 plates at the end to ensure good shower containment. Laterally it extended over a surface of 240 × 240 cm^2. This resulted in a fiducial mass of 87 t.

3.2.1 Data taking. The detector was exposed to neutrino and antineutrino beams; part of the time a dump block was inserted into the beam to determine the WB background.

The number of protons on target (p.o.t.) collected for each of these settings is given in Table 2. Additional data were taken with the Cherenkov counter in the beam to measure the pion and kaon composition.

Protons were extracted from the SPS in bursts with a bell-shaped time structure, approximately 500 µs wide at the base. This spill-width was chosen as a compromise between excessive detector dead-time on the one hand and a large cosmic-ray background on the other hand. A 750 µs gate (GATE 1) was used at the ejection-time to include the spill-width and small drifts in the timing of the ejection.

In addition to this gate covering the extraction-time, events were also accepted in a second gate (GATE 2), which was opened after the end of the proton spill. GATE 2 was 3 times longer than GATE 1 and provided a measurement of the cosmic-ray background in the neutrino triggers. This gating structure was repeated for every SPS cycle with a cycle time of 12 s.

3.2.2 Trigger. The trigger logic was based on scintillator information with a discriminator threshold set to $\frac{1}{5}$ of the average energy deposition of a minimum ionizing particle.

The trigger requires at least one hit recorded in

at least four scintillator planes with the requirement of no hit in the first plane to veto incoming charged particles. This condition corresponds to a minimum energy deposition of 1.5 GeV for showers. The efficiency of the trigger will be discussed in a later section.

3.2.3 Selection of valid bursts. Beam-monitor information was made available to the one-line system in the form of direct pulse trains ('hardware information') and was also transmitted through the Neutrino Facility Monitor computers in the form of blocks of data ('software information').

Software information was used to define conditions for rejecting bad quality bursts. The thresholds for these cuts were fixed for long periods during which the running conditions were stable.

Intensity and position of the extracted proton beam as well as of the secondary hadron beam were thus constrained to stay within acceptable limits. Bursts with insufficient monitoring information (mainly due to failures in data transfer) were also rejected.

The percentage of protons on target rejected after the cuts for each running condition and the percentage effectively used in the analysis are given in Table 2.

3.2.4 Suppression of 'double events'. The process of digitization of events in the proportional drift-tube system has an active gate length of ≈ 1 μs. Because of this gate width a few per cent of the events occur together with a second event within the same conversion-time.

For each event the time which elapsed between the trigger and the next interaction was recorded with a time-to-digital converter (TDC). The time measurement was started 200 ns after the trigger and was stopped by the following interaction which released a total energy larger than ≈ 1.5 GeV. The time was digitized in 50 ns intervals. Events followed by another interaction in a time window of 200 to 1200 ns were rejected in the analysis. Most of the problems due to pattern recognition introduced by overlay events were removed in this way.

The procedure introduces an additional 'dead-time' of $\approx 2\%$, which, however, does not affect the measurement of R^v. This dead-time was determined by the fraction of events with TDC counts in a time window from 1200–2200 ns (see Fig. 4). Since the spill structure is nearly constant on a microsecond scale, the number of events rejected in the window from 200–1200 ns should be equal to the number of events found in a window of equal width following it. The data presented in Fig. 4 shows that the recognition efficiency for CC events is significantly affected by
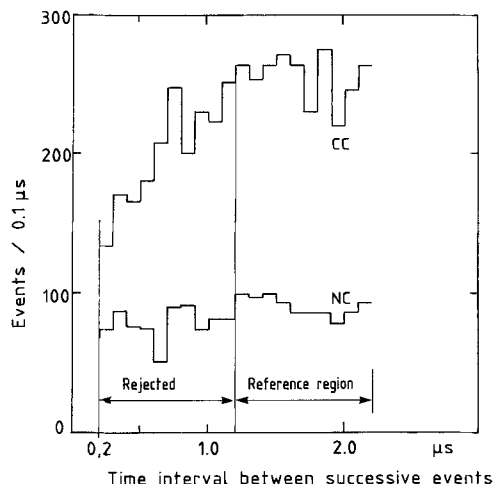

Fig. 4. Rejection of 'double events'

the presence of a second interaction; the event rate is normally expected to be flat in Δt, as in the case for $\Delta t > 1.2$ μs. The inclusion of the events occurring in the region labelled 'rejected' would therefore introduce an error in the measurement of R^v.

3.2.5 Relative normalization of different running conditions. In order to subtract cosmic-ray background the exposures during GATE 2 had to be normalized relative to the respective exposures during GATE 1 for the four data-taking conditions. This normalization is performed by measuring the integrated gate length with a clock, taking the detector dead-time into account.

The subtraction of WB background requires a relative normalization of normal running compared to 'dump' running. This normalization is done on the basis of the integrated intensity of the secondary hadron beam, measured just ahead of the entrance of the decay tunnel. The intensity is measured with the beam-current transformers (BCTs) described before. The dead-time of the neutrino detector was taken into account weighted with the spill-time structure of the proton extraction. A small correction was applied for protons extracted at times outside the neutrino detector gate, but measured in the BCT gate ('gate inefficiency').

The relative normalization of the neutrino exposure with respect to the antineutrino exposure was performed with the help of a measurement of the integrated muon flux in the shielding obtained with the system of solid-state detectors (SSDs). Dead-time corrections weighted with the spill-time structure and corrections for 'gate inefficiency' were applied. The relative muon fluxes are closely related to the relative neutrino fluxes; only small corrections have to be made. Had the measured secondary hadron beams

Table 3. Systematic errors on the ν_μ and $\bar{\nu}_\mu$ flux ratio (%)

Source	Error on flux ratio (%)
Monte Carlo statistics	1.0
K/π ratio	0.9
Beam width	0.2
Beam steering	0.1
Vertex resolution	0.1
Muon tracking	0.4
SSD position	0.5
Trapped muons	0.7
SSD stability	1.0
Dead-time	0.5
Total error (sum of squares)	2.0

been chosen for this purpose larger uncertainties would have been introduced by the need to correct for the proton, pion, and kaon fractions in the positive and negative secondary beams.

After subtraction of the background muons coming from π and K decays upstream of the decay tunnel ('trapped muons'), the SSDs measure the sum of the signal of muons produced by π and K decays. The ratio of the SSD signals in ν and $\bar{\nu}$ running determines the relative pion and kaon rates in these exposures; the ratios K^+/π^+ and K^-/π^- were determined by a Cherenkov counter and the acceptance of the counters for measuring a muon from pion and kaon decay in the beam was calculated by Monte Carlo simulation. The sum of the signals of a system of detectors placed on a ring with 15 cm radius around the nominal beam axis at a depth of 30 m of iron was used for this normalization. This procedure minimizes the effects of variations in the steering of the beam. From the relative pion and kaon fluxes in the two exposures the neutrino to antineutrino flux ratio can be obtained. The acceptance for measuring muons in the counters was calculated with a Monte Carlo program, simulating the NBB line to obtain the phase-space densities of pions and kaons and of the daughter particles produced in their decays. The muons were tracked through the iron shielding and the acceptance for their detection with the SSDs was determined. The neutrinos were followed up to the neutrino detector to determine the corresponding neutrino flux ratio. The uncertainties in the determination of the ratio of the antineutrino and the neutrino fluxes are listed in Table 3.

3.2.6 Dead-time correction. The dead-time of the detector was measured using a 1 MHz clock during the active time of the detector and during the integrated gate-time. This procedure gives an accurate sampling

of the unweighted dead-time needed for subtraction of cosmic-ray background.

The flux-weighted dead-time was measured using signals from small scintillators inserted into the muon shield after ≈ 120 m of iron. These scintillators had a cross-section of 0.1 cm^2 perpendicular to the beam and counted the beam related muon flux at a rate of about 100 kHz. The signals of these scintillators were counted during the active time of the detector (A), during the neutrino detector gate (G), and during a wide gate (W), around the proton extraction time. The probability of recording a muon signal in these scintillator counters is proportional to the neutrino flux at that time; therefore the use of these signals makes it possible to measure the flux-weighted dead-times. The expression $1 - A/G$ determines the flux-weighted detector dead-time, and $1 - G/W$ the 'gate inefficiency'.

Average weighted and unweighted dead-times are reported in Table 2; the effective dead-time introduced by the procedure used to reject double events is also given.

3.2.7 Fast cosmic-ray filter. In order to reduce the background of cosmic-ray events and consequently to reduce the statistical error when subtracting the background, a filter program was used, which consisted of two stages.

The first stage removed $\approx 80\%$ of the cosmic-ray events, which were those with tracks entering the detector from the front face or from the side faces travelling in the beam direction; it was checked that it did not reject neutrino-induced events. Tracks were defined by hits in the proportional tubes and allowance was made for one extra noise hit.

The second stage was more sophisticated and after this stage only one out of 2000 cosmic-ray triggers survived, reducing the trigger rate of 4 kHz to a few per second. This rejection rate is achieved by an efficient suppression of tube hits which are not related to the event ('noise') and by the use of scintillator as well as proportional tube information. On the basis of local patterns, active elements are classified as 'shower-hits' or 'track hits'. Events with shower hits are not rejected. For the remaining events it was checked whether the hits, grouped in clusters, were connected to form an entering track. The cluster sizes were checked for consistency with the track angle. Such events were rejected too.

This algorithm has a small inefficiency for accepting neutrino-induced NC events, which will be quantified in the following section.

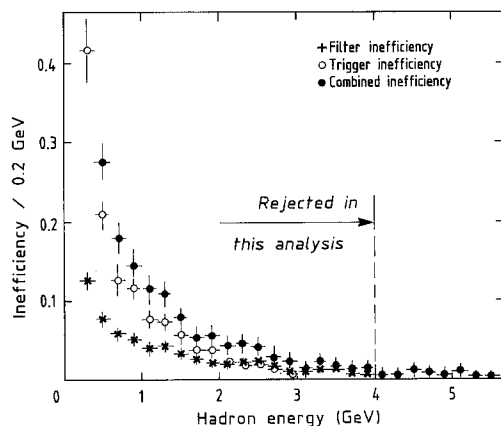*3.2.8 Trigger and filter inefficiencies.* A priori, a lower triggering efficiency has to be suspected for NC events

618

Fig. 5. Trigger and filter efficiencies

Fig. 6. Efficiency near the veto plane

compared to that for CC events, because of the absence of a charged primary lepton track. The potential loss is expected to increase for decreasing shower energy. To study this effect we used the observed CC event sample. A new sample of 'pseudo NC events' was created by removing the muon in each CC event. This procedure was performed by the code of the reconstruction program. Particular care was taken to recalculate the scintillator pulse heights by subtracting the expected muon contribution along the muon track. The calculated scintillator pulse heights were used to determine whether the 'pseudo NC' event satisfied the trigger requirements. The fraction of lost events per hadron energy bin is reported in Fig. 5.

The fraction of these pseudo NC events rejected by the cosmic-ray filter is also given in the figure. The correlation between the two effects is small and the total loss is approximately equal to the sum of the two individual losses. The combined inefficiency for NC events as a function of hadron energy is also shown in Fig. 5. For hadron energy above 4 GeV the integrated inefficiency amounts to $(0.2 \pm 0.1) \times 10^{-3}$ for neutrino events and $(0.4 \pm 0.4) \times 10^{-3}$ for antineutrino events.

3.2.9 Efficiency near the veto plane. Back-scattering may have a different effect on the veto efficiency for NC and CC events. We determined that efficiency using NC and CC events produced in the centre of the fiducial volume. A sample of 'pseudo NC events' was created by shifting the longitudinal vertex coordinate (plane number) towards the veto plane. The reconstructed scintillator pulse heights were used to determine whether the 'pseudo NC event' satisfied the veto criteria. The ratio of events accepted by the veto condition is reported in Fig. 6 as a function of plane number for NC and CC events. Integrating the efficiency over the fiducial volume we find a difference
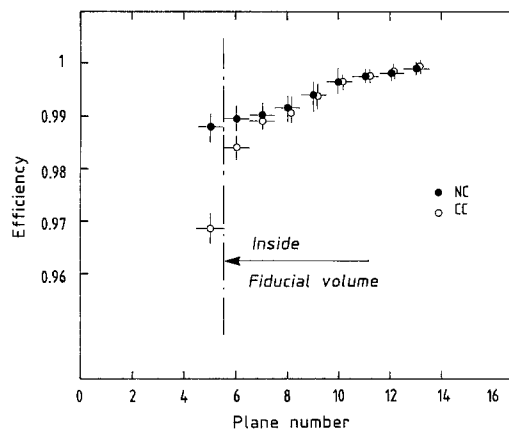
for CC and NC events $< 10^{-4}$. This difference has been taken into account in the analysis.

4 Analysis

The analysis was performed in several steps. First, events were separated into classes of NC and CC candidates, then corrections were applied for event loss and background to obtain the physical NC and CC event numbers.

4.1 Event recognition

Interactions in the CHARM detector were classified by an automatic pattern-recognition program on an event-by-event basis. Selection criteria were applied which attempt to identify optimally the physical processes and to minimize the corrections needed to relate the visible cross-sections to the physical cross-sections.

4.1.1 Classification criteria. Neutrino interactions were defined as events which have no entering charged tracks.

A neutrino event is classified as a CC interaction if it contains a muon originating at the event vertex. A muon is assumed to originate from the event vertex if its extrapolated intercept with the vertex plane of the event lies within 30 cm of the measured shower vertex, or if sufficient energy is measured in a box around the extrapolated point. Muons have to be seen in the 140 ns scintillator gate following the trigger to ensure suppression of overlay tracks seen in the proportional-tube system, which has an effective gate length of ≈ 1 μs. The muon has to be visible over a range corresponding to an energy loss of at least 0.67 GeV. Its total range has to exceed 1 GeV energy loss, corresponding to a penetration of 20 calorimeter
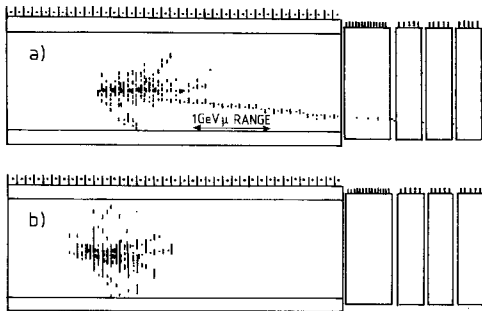
Fig. 7. a Typical neutral-current and **b** typical charged-current events recorded in the CHARM detector

planes. The visible range of a muon track is defined as the length, measured in equivalent range, between the first clearly visible point outside the shower and the last point on the track, as seen by the proportional-tube system. Tube hits are deemed to be clearly visible points on a track if they are separated laterally by at least 5 quiet tubes from their neighbouring hits (15 cm isolation criterion). In addition they are required to be isolated from other hits which do not belong to the muon track, in the longitudinal direction. These isolation criteria are much more strict than the ones used in a previous publication on the same subject [7] and tend to reject more tracks on the basis of the requirement of 0.67 GeV visible range.

All other neutrino-event candidates are classified as NC interactions. Only those events with a vertex inside the fiducial volume and with shower energy of at least 4 GeV were analysed further. It was checked that no bias was introduced by these cuts in the NC to CC event ratio. Representations of a typical NC and a typical CC event in the CHARM detector are shown in Fig. 7.

In order to obtain the CC and NC event numbers from the automatic classification, the following corrections have to be applied to the event numbers:

    i) classification inefficiencies of the automatic reconstruction program,

    ii) loss of muons not satisfying the selection criteria,

    iii) π and K decays in the shower faking a primary muon,

    iv) v_e background produced by K_{e3} decays in the beam,

    v) cosmic-ray background and WB background

These corrections will be discussed in the following subsections.

4.1.2 Classification inefficiency. The program recognized and flagged event topologies for which the automatic procedure could fail. Events were selected for scanning before the energy and fiducial volume cuts

Table 4. Classification matrix of a sample of 5% of the data. Horizontal rows give the program classification; vertical columns give the scanning classification. Events are classified as CC, NC, and events outside the fiducial volume (OCC, ONC)

	CC	NC	OCC	ONC
CC	5669	1	0	0
NC	1	2171	0	0
OCC	3	0	2728	0
ONC	0	2	0	1593

and the cut on the 'double-event' TDC were applied in order to check the systematic biases introduced by them. Approximately 1% of all neutrino triggers after rejection of the cosmic-ray events by the filter were flagged as events for which it is difficult to reconstruct the topology automatically. Typical cases are:

    i) tracks which fail the vertex extrapolation because of random association of shower hits to the track resulting in a bad straight-line extrapolation to the vertex;

    ii) tracks for which the scintillator timing criteria are not fulfilled owing to geometrical or electronic inefficiencies;

    iii) multiple track events for which the matching of the two projections of the primary muon is difficult;

    iv) events with inconsistencies in the vertex-finding algorithm, producing two incompatible estimates for the vertex position.

These flagged events were visually inspected in a double scan and corrected on an event-by-event basis. Roughly 600 events out of a total of 4000 flagged events were reclassified. The scanning efficiency for this category of events was found to be >99%.

In addition to these flagged events a randomly selected sample totalling 5% of all triggers which survived the cosmic-ray filter were scanned in order to determine the inefficiency of the automatic pattern-recognition program and to correct for it on a statistical basis. The double scan showed that, after applying the energy and fiducial volume cuts, 7 events in this sample were misclassified (Table 4). A global correction for this classification error was then made; it introduced an uncertainty of $\Delta R^v/R^v < 0.1\%$.

4.1.3 Muon-recognition losses. Charged-current events in which the primary muon cannot be identified are by definition classified as NC. Some of these lost CC events have a muon with an energy of less than 1 GeV. Another contribution to the loss of CC events is caused by muons of more than 1 GeV either leaving the sides of the detector before depositing sufficient energy, or being obscured by the hadronic shower. The two categories are of approximately
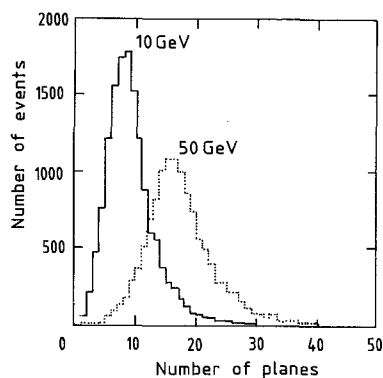
620

Fig. 8. Effective hadron shower length

Fig. 9 a, b. Comparisons between Monte Carlo simulation and data of shower-energy distribution a and event radius b of CC events

equal importance. A correction is required for these CC losses. As this is the largest correction required, the precision which can be reached in measuring R^ν depends in an essential way on the reliability of estimating these losses. To test our methods we determined the correction in two independent ways. Both methods do not require a simulation of hadronic showers, a notoriously difficult enterprise.

For the first method, real CC events were used in order to reproduce the properties of hadronic showers, and their primary muon tracks removed. Only events for which the primary track was well reconstructed were used in this analysis. This selection introduces a small bias in the shower-energy spectrum, which is corrected for in the subsequent analysis by calculating the correction as a function of the shower energy. In a second step, a simulated muon is merged with the original shower. The direction and momentum of the muon are chosen randomly in such a way as to agree statistically with the expected distribution from the NBB. The muon-reconstruction efficiency is obtained by passing these 'semi Monte Carlo' events through the standard analysis chain.

A second method was developed in which the hadronic shower properties were determined from CC events. The 'effective' length of showers was obtained by measuring for each recognized CC event the distance between the shower vertex and the first point of the muon track which is clearly visible outside the shower. Histograms were made of these distances as a function of the relevant kinematic variables, namely the shower energy and the opening angle between the muon and the shower. Typical shower-length distributions for 10 and 50 GeV hadron energies are shown in Fig. 8.

These histograms were used to determine the invisible part of simulated muon tracks. These tracks were simulated taking all details of the detector into account and the selection criteria were then applied in order to determine the efficiency. The agreement
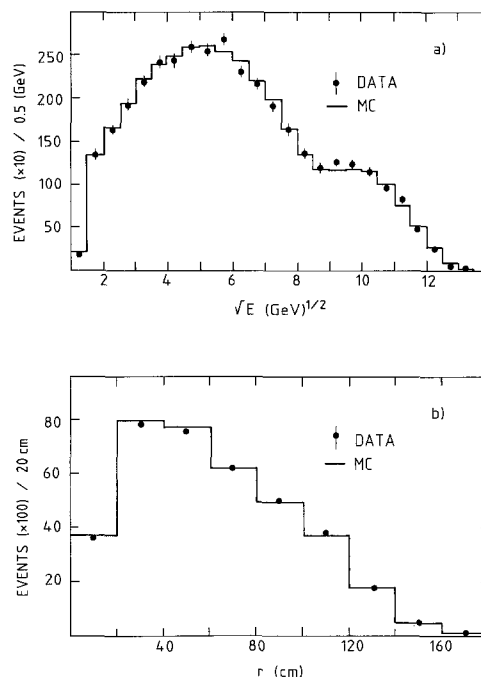
between data and the pseudo Monte Carlo events is very good; Fig. 9a and b by show the comparison for the shower-energy distribution and for the distribution of event radius with respect to the beam axis. Comparisons of average hadron shower length with hadron shower energy (a) and measured muon total range distribution (b) are shown in Fig. 10.

The total inefficiency of the selection criteria for muons is calculated to be 3.5%. Its variation with the generated muon momentum is shown in Fig. 11. The two methods give a consistent result to within 2% of the correction.

The uncertainty of the parent-beam momentum and that of the muon momentum measurement by the CHARM detector introduce systematic errors in the correction. In order to largely eliminate these systematic errors in the calculation of the correction we defined a 'reference region' of muon momentum and normalized lost muons to the event number found in this region. Charged-current events with a primary muon of 3–5 GeV energy were accounted for in the reference region. The ratio of all CC events with an unseen muon and of identified CC events in the reference region was then calculated using the Monte Carlo program described above. The absolute number of CC events for which the muon was not recognized is obtained by multiplying this ratio with the actual number of CC events found in the reference region. Contributions from background events in the reference region were also taken into account. This proce-
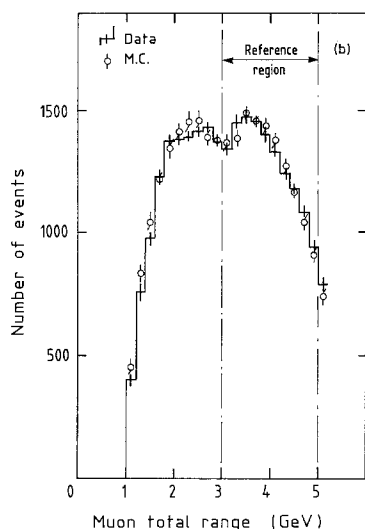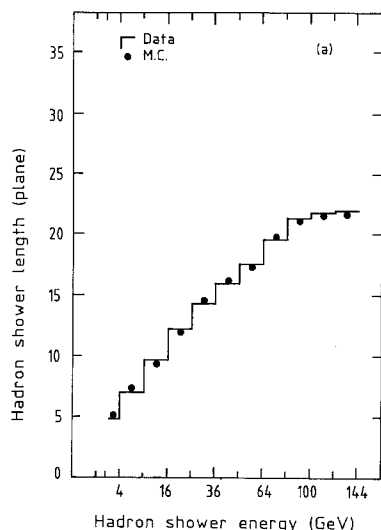
Fig. 10a, b. Comparison between Monte Carlo simulation and data of average hadron shower length versus hadron shower energy **a** and distribution of measured muon total range **b** of CC events
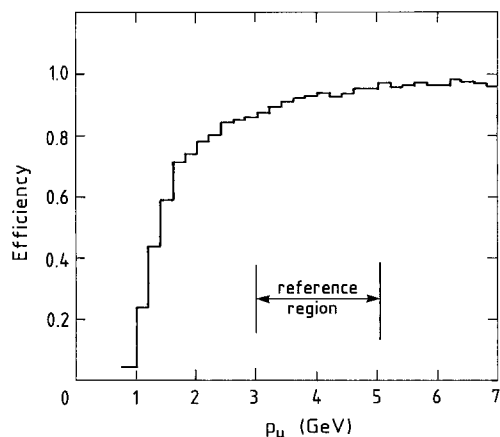

Fig. 11. Muon-finding efficiency

dure eliminates all errors introduced by uncertainties in the beam energy, the energy loss of muons, the density of the detector, and the slope of the y-distribution. This cancellation is exact for all such scale errors because the simulated events in the reference region scale with the number of events with lost muons. The remaining systematic error is dominated by the uncertainty in the determination of the shower length (± 0.5 calorimeter plane) and is estimated to be $\pm 2.8\%$ of the correction corresponding to $\Delta R^{\nu}/R^{\nu} = 0.32\%$. In the calculation of the effect of lost primary muons it was taken into account that in such CC events a secondary muon can be recognized as a primary muon ('π/K-decay correction').

4.1.4 π and K decays in showers and punch-through tracks. A fraction of NC events containing a track which fulfils the requirements of a primary muon of a CC event are classified as CC events. This background is caused by decays of pions or kaons in the shower or by punch-through tracks.

We calculated this correction by using again events detected in the experiment. Charged-current events with well-measured primary muons were selected and the muon removed; the remainder of the event was then processed through the standard analysis chain. A second track fulfilling the conditions for a primary muon was searched for in these events.

The fraction of events for which a second muon was found then determined the correction to be applied. In the selected sample [6.02±0.08(stat.) ±0.04(syst.)]% of the events had a second track satisfying the primary-muon criteria. The systematic error includes biases introduced by the fact that in a small number of events the original primary muon cannot be perfectly removed.

However, the sample of showers obtained from CC events has some differences with respect to the NC events, which have to be taken into account. In a fraction of CC interactions, a second prompt muon in the shower comes from charm-quark production and subsequent semileptonic decay. Neutral-current interactions do not change the flavour of quarks and this effect is therefore absent in these interactions. The corresponding events must be subtracted from the event sample. This amounts to (0.54±0.08)% of the selected sample. Charm production from d and s quarks and its semileptonic decay into muons is modelled in a Monte Carlo program; the rate is determined by the ratio of dimuon and single-muon events produced by neutrinos found in the literature [18]. The model for charm production described thresholds by the so-called slow rescaling approximation with a charm-quark mass $m_c = 1.5$ GeV [19]. The acceptance was calculated using a flat fragmentation func-
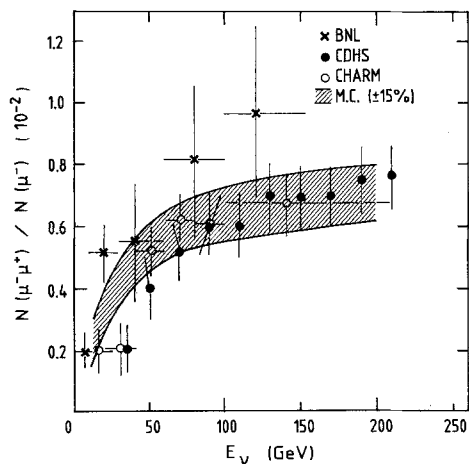
Fig. 12. Dimuon production by neutrinos. Comparison of the model with data

Fig. 14. Typical Cherenkov pressure curve in the neutrino beam
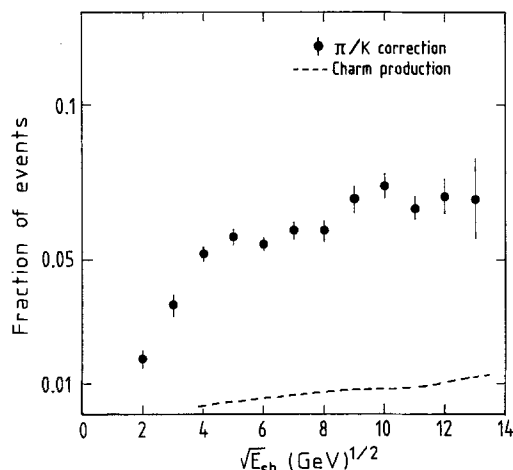

Fig. 13. π and K decay correction

tion. The agreement with available data is shown in Fig. 12. An uncertainty of $\pm 15\%$ is assumed for the absolute normalization of the subtraction (shaded areas in Fig. 12).

Strange particles are produced more frequently in NC events than in CC events. This leads to a larger contribution of decays of primary shower particles in NC events. The calculated correction is $(0.04 \pm 0.02)\%$.

In order to avoid biases introduced by the selection of the CC events used to determine the fraction of showers with two primary muons, the correction is applied as a function of the shower energy (Fig. 13). We also verified whether the selection of events, with well-measured muon tracks used to determine the correction did not introduce a change in the final fraction of events found with a second primary muon. However, a small contamination of the sample by
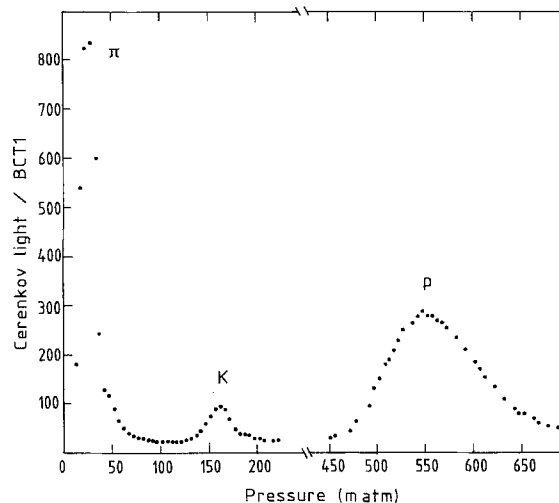
NC events with a well-measured muon track has no effect on the final result.

The magnitude is significantly higher than that of the equivalent correction applied during the analysis of previous data [7], because in the present case no attempt was made to remove pion tracks from the primary muon sample on the basis of hadron-like behaviour.

4.1.5 Electron-neutrinos produced in the NBB. Both NC and CC interactions of electron-neutrinos originating from K_{e3}-decays are classified as NC events. The contribution of these events amounts to 6.6% of the NC candidates in the v exposure and 4% in the $\bar{v}$ exposure.

To calculate the correction, the ratio of kaons to pions in the beam had to be determined; it was measured using a focusing gas Cherenkov counter which was moved in the beam, near the hadron dump, for special runs. Figure 14 shows a typical Cherenkov pressure (P) curve. The peaks in the region $0 < P < 110$ matm, $135 < P < 210$ matm and $450 < P < 750$ matm correspond to π, K, and p signals, respectively. The background was interpolated from the regions outside the peaks, assuming a linear variation. The measurements yielded the ratios:

$K^+/\pi^+ = 0.1282 \pm 0.0006\,(\text{stat.}) \pm 0.0027\,(\text{syst.}),$

$p/\pi^+ = 1.628 \pm 0.005\,(\text{stat.}) \pm 0.070\,(\text{syst.}),$

$K^-/\pi^- = 0.0630 \pm 0.0011\,(\text{stat.}) \pm 0.0030\,(\text{syst.}),$

$\bar{p}/\pi^- \leq 1.3\%\,(90\%\ \text{CL}).$

The statistical errors are derived from the dispersion of the values obtained in different runs. The systematic errors are due to the uncertainties in the estimation

of the background and in the definition of the π and K regions. The contamination of the pion peak by positrons and electrons was estimated to be <0.87% and <1.3% at 90% CL, respectively, for the ν and $\bar{\nu}$ beams and was substracted.

The number of ν_e-induced events was calculated assuming e-μ universality of the weak interaction in the context of the Standard Model.

A small correction was applied for events with showers generating a decay muon, causing these events to be classified as CC events. Using the measurement of the K/π ratio with an error of $\pm 3\%$, this correction was calculated to $\pm 4\%$ of its value, corresponding to $\Delta R^\nu/R^\nu = 0.3\%$.

4.1.6 Wide-band background.
The neutrino flux from pion and kaon decays before the decay tunnel and before the momentum and charge selection is not easily calculable, and it is therefore preferable to measure it separately by blocking the entrance of the decay tunnel with a dump.

The procedure was to define all of the neutrino flux generated before the dump as background and the flux from decays downstream of the dump as 'beam'. The relative normalization of the periods when the dump blocked the entrance of the decay tunnel with respect to the standard running conditions was performed using the signal of the secondary hadron BCT. The uncertainty introduced by this WB background amounts to $\Delta R^\nu/R^\nu = 0.3\%$.

In normal running conditions the hadron beam is dumped at the end of the decay tunnel. In special runs with a dump at the entrance of that tunnel, the hadron beam is dumped there. The different location of the hadron dump has three consequences:

i) It introduces a different detection acceptance for the neutrinos created in the dump.

ii) The finite amount of gas in the 300 m long 'vacuum' acts as a target for secondary hadrons during normal data taking and neutrinos created in subsequent decays are not subtracted when the subtraction procedure is applied.

iii) The finite length of the special dump (1.5 m Fe or ≤ 8 interaction lengths) makes it necessary to apply a correction for non-containment and subsequent decay into neutrinos of secondary particles created in the dump and escaping from it.

Table 5 shows the background contamination expected in the detector for each condition of running. Errors are statistical only. The corrections were included in the WB background.

4.1.7 Cosmic-ray background.
The uncertainty introduced by the cosmic-ray background during normal data taking is small, because sufficient data were tak-

Table 5. Contamination from dump and other sources

	ν	ν-dump	$\bar{\nu}$	$\bar{\nu}$-dump
From dump ($\times 10^{-3}$)	–	4.1 ± 2.1	–	1.3 ± 0.7
From rest gas ($\times 10^{-5}$)	2.2 ± 1.0	–	2.0 ± 1.0	–
From shielding at end of decay tunnel ($\times 10^{-5}$)	11.0 ± 1.2	–	9.0 ± 1.0	–
Total ($\times 10^{-3}$)	0.13 ± 0.02	4.1 ± 2.1	0.11 ± 0.2	1.3 ± 0.7

en in periods without beam to measure the correction and also because the correction is rather small. The cosmic-ray contribution to CC events is negligible and is 1% of the NC sample in the neutrino beam, and 4% of the NC sample in the antineutrino beam.

4.2 Determination of the cross-section ratios

The ratio of NC to CC events and the $\bar{\nu}$ to ν CC cross-section ratio were determined for different values of the cut in hadron energy. This makes it possible to study the dependence of the value of $\sin^2 \theta_W$ on the hadron energy cut.

The corrections applied to obtain the sample of physical events in the neutrino beam are given in Table 6 for a 4 GeV hadron energy cut. The effects of mixing of NC and CC events and the subtraction of ν_e-induced events from K_{e3} decays in the beam are also given. The results for the antineutrino data are given in Table 7.

A correction for a small deviation from isoscalarity of the target material was applied to the ratios of NC to CC events to derive the cross-section ratios, R^ν and $R^{\bar{\nu}}$. For the ratio r of the total antineutrino and neutrino CC cross-sections, r, an additional cor-

Table 6. Event numbers for neutrino exposure ($E_h \geq 4$ GeV)

	NC	CC
Uncorrected data sample	39239 ± 198	108472 ± 329
Trigger + filter efficiency	7 ± 4	0 ± 0
Scan correction	40 ± 40	60 ± 44
Corrected raw data sample	39286 ± 202	108532 ± 332
WB and cosmic correction	-2310 ± 87	-4311 ± 119
– of which WB	-1998 ± 88	-4308 ± 119
– of which cosmic	-312 ± 8	-3 ± 1
Clean NBB data sample	36976 ± 225	104220 ± 361
Possible difference in energy cut for NC and CC	–	0 ± 129
Lost muons	-3737 ± 105	3735 ± 105
π and K decay	1893 ± 50	-1835 ± 50
K_{e3} CC	-1768 ± 68	-106 ± 6
K_{e3} NC	-532 ± 20	-33 ± 2
Corrected event numbers	32831 ± 283	105981 ± 408

Table 7. Event numbers for antineutrino exposure ($E_h \geq 4$ GeV)

	NC	CC
Uncorrected data sample	2314 ± 48	5455 ± 74
Trigger + filter efficiency	1 ± 1	0 ± 0
Scan correction	0 ± 0	0 ± 0
Corrected raw data sample	2315 ± 48	5455 ± 74
WB and cosmic correction	-368 ± 26	-450 ± 29
– of which WB	-275 ± 26	-449 ± 29
– of which cosmic	-93 ± 3	-1 ± 0
Clean NBB data sample	1947 ± 55	5005 ± 79
Difference in energy cut	–	0 ± 16
Lost muons	-45 ± 5	45 ± 5
π and K decay	104 ± 5	-98 ± 6
K_{e3} CC	-56 ± 3	-3 ± 1
K_{e3} NC	-19 ± 1	-1 ± 0
Corrected event numbers	1931 ± 58	4948 ± 81

Table 8. Ratios R^ν, $R^{\bar\nu}$ and r for two E_h thresholds

E_h cut	R^ν	$R^{\bar\nu}$	r
4 GeV	0.3093 ± 0.0031	0.390 ± 0.014	0.456 ± 0.011
9 GeV	0.3052 ± 0.0033	0.397 ± 0.015	0.429 ± 0.010

Table 9. Mass thresholds

Final-state quark	CC	NC
u or d quark	$m_N + m_\pi$	$m_N + m_\pi$
s quark	$m_N + m_K$	$m_N + 2m_K$
c quark	$m_N + m_D$	$m_N + 2m_D$

5.1 Radiative corrections

We applied radiative corrections to R^ν, $R^{\bar\nu}$, and r, following Bardin et al. [20], in the on-shell renormalization scheme of Sirlin [21]. In this scheme the calculable electroweak observables can be expressed in terms of the following set of independent quantities:

i) α, the fine structure constant at m_μ^2 ($\alpha^{-1} = 137.035963$);

ii) G_F^μ, the Fermi constant in μ decay ($G_F^\mu = 1.16637 \times 10^{-5}$ GeV^{-2});

iii) m_Z and m_H, the physical masses of the Z^0 and Higgs bosons;

iv) (m_i), the set of fermion masses.

$\sin^2 \theta_w$ is defined from the measured W and Z masses (e.g. in $p\bar p$ colliders) by the expression:

$$\sin^2 \theta_W = 1 - m_W^2/m_Z^2.$$

The theoretical uncertainty on $\sin^2 \theta_W$ due to the unknown value of the mass of the top quark (30 GeV/c$^2 < m_t < 240$ GeV/c^2) and of the Higgs boson (10 GeV/c$^2 < m_H < 1000$ GeV/c^2) is estimated to be ± 0.0015 [22]. In the calculation the top and Higgs masses were set to 45 GeV and 100 GeV, respectively.

One-loop electroweak radiative corrections were calculated using a set of computer programs made available to us by Bardin. The calculation was done in four step.

The double differential cross-sections $d^2\sigma/dx\,dy$ for scattering of $\nu(\bar\nu)$ off individual quarks are first calculated up to one-loop corrections. The initial quark momentum is then replaced by ξp_N, where ξ is the fraction of nucleon four-momentum p_N carried by the parton; ξ is the Nachtmann definition of the scaling variable taking the finite target mass into account.

The cross-sections were then multiplied by the parton distribution functions $f(\xi)$ of individual quarks given by Barger and Phillips [23], integrated over ξ and incoherently summed for all types of quarks involved in the reaction.

Diagrams of internal bremsstrahlung can generate real photon emission. Owing to the detection method, the energy of these photons adds to the shower energy. We took the relative detector response to electromagnetic and hadronic showers in the ratio of 1.17 into account [17] in calculating this part of the radia-

rection for the different spectra in neutrino and antineutrino exposures was applied. This is because, Eq. (9) being formulated in terms of differential cross-sections, any integrated cross-section satisfies the equation for arbitrary regions in x and y, provided the integral is taken over the same neutrino and antineutrino spectrum.

The measurements of R^ν, $R^{\bar\nu}$, and r are given for 4 and 9 GeV hadron energy cuts in Table 8.

5 Determination of $\sin^2 \theta_W$

The electroweak mixing angle was deduced from (10). It is valid for an isoscalar target containing only u, $\bar u$, and d, $\bar d$ quarks without quark mixing and must therefore be corrected for contributions from s and c quarks in the nucleon and for c quark production by quark mixing. These corrections were determined in the context of the quark model of the nucleon. Quark mixing was described by the Kobayashi-Maskawa matrix.

We applied radiative corrections to the ratios of the cross-sections, R^ν, $R^{\bar\nu}$, and r.

Quark fragmentation in the final state of deep inelastic neutrino scattering leads to thresholds in the invariant mass which depend on the quark content of the reaction (see Table 9). The muon mass is explicitly taken into account in the expression for the CC reaction.

tive corrections. The effective energy threshold (4 GeV) for CC events is shifted with respect to that for NC events.

Finally, a weighted average of cross-sections over protons and neutrons was calculated.

Tables of corrections to NC and CC double differential cross-sections were produced and integrated over the experimental conditions using a linear interpolation method. The correction to $\sin^2 \theta_W$ is -0.0092.

It must be pointed out that the calculation of radiative corrections to semi-leptonic neutrino interactions is model dependent owing to the somewhat arbitrary choice of structure functions used and the initial and final quark-mass dependence. Bardin et al. checked that the dependence on the structure functions was weak. They also studied the effect of a variation of the final quark masses between 1 MeV and 1 GeV and found that it changed the corrections on CC and NC cross-sections by less than 1%.

The radiative corrections were also calculated using computer programs made available to us by Roos et al. [24]. This calculation was performed using different structure functions and gave a correction to $\sin^2 \theta_W$ of -0.0122. More calculations were done by other groups [11] taking into account similar experimental conditions. They give reasonable agreement with the previous ones. We therefore estimate an uncertainty on the correction of $\Delta \sin^2 \theta_W = \pm 0.002$.

5.2 Quark-model corrections

The ratio of the contributions to the cross-sections given by scattering off antiquarks and quarks was modelled by requiring consistency with the measurement of r in the analysis: we found

$$\bar{q}/q_v = 0.19 \pm 0.02,$$

where $\bar{q}$ and q_v denote, as usual, the momentum weighted contents of antiquarks and valence quarks in the nucleon, respectively. We described the strange-quark sea using experimental data on neutrino-induced dimuon production [25] and used

$$\bar{s}/d_v = 0.06 \pm 0.02.$$

Following [26], we parametrized the x dependence of the strange sea by the expression

$$s(x, Q^2) = A(1-x)^B + C \exp(-Dx),$$

using Q^2-dependent values of the parameters A, B, C, and D. For $Q^2 = 5$ and 20 GeV^2 the parameters are given in Table 10. This parametrization is consistent with the dimuon analysis of [25].

Table 10. Strange sea parameters

Parameter	$Q^2 = 5$ GeV^2	$Q^2 = 20$ GeV^2
A	0.0551	0.0933
B	6.3907	7.1820
C	0.0671	0.0637
D	13.21	16.12

For the charm-quark sea we used

$$c/s = 0.2 \pm 0.2$$

as derived from dimuon production by deep inelastic muon scattering [27]. In flavour-changing reactions $(d \to c, s \to c)$ we described the kinematical threshold effects introduced by the c quark mass m_c using the so-called slow rescaling model [19] with a fixed value of $m_c = 1.5$ GeV/c^2. This mass is not directly determined from measurements and has an uncertainty which is estimated to be ± 0.3 GeV/c^2. This is the largest theoretical uncertainty affecting $\sin^2 \theta_W$ derived from (10). We therefore give $\sin^2 \theta_W$ for this central mass value and a linear approximation valid in the range 1 GeV/c$^2 < m_c < 2$ GeV/c^2. We hope that further progress on determining m_c can be made, thus enabling a more precise determination of $\sin^2 \theta_W$.

We used values of the Kobayashi-Maskawa (K-M) mixing matrix derived assuming three families of quarks and requiring unitarity of the matrix [28].

Finally, we corrected (10) for effects due to the longitudinal structure function F_L and used a parametrization consistent with QCD predictions and with available measurements [13].

Higher twist effects are claimed to be small [12]; nevertheless, we investigated their effects by varying the hadron energy cut from 4–9 GeV (see Subsect. 5.4).

5.3 Discussion

The different corrections applied to obtain $\sin^2 \theta_W$ from R^v and r measured with a 4 GeV energy cut are given in Table 11. Although the net correction is small, it is made of large single contributions.

An estimation of the uncertainties introduced by the model-dependent corrections ('theoretical uncertainties') is also given. The major part of the uncertainties is introduced by the uncertainty in the c-quark mass m_c. The uncertainty in the normalization of the s-quark component of the cross-section cancels to a large extent for values of m_c near 1.5 GeV, because it contributes comparable fractions to the NC and CC cross-sections.

Table 11. Corrections to $\sin^2 \theta_W$ ($E_h \geq 4$ GeV)

Source	$\Delta \sin^2 \theta_W$	Theoretical uncertainty
Muon mass	+0.0011	±0.0001
W^2 thresholds, F_L	+0.0005	±0.0005
K-M mixing matrix		±0.0010
Strange sea for $m_c = 0$	−0.0074	±0.0010
Charm sea for $m_c = 0$	+0.0015	±0.0010
Radiative corrections	−0.0092	±0.0020
Total uncertainty (fixed m_c)		±0.0030
Charm mass ($m_c = 1.5$ GeV/c^2)	+0.0140	
Total ($m_c = 1.5$ GeV/c^2)	+0.0005	±0.0030

5.4 Results

Applying both quark-parton model (qpm) and radiative (rad) corrections, we obtain the final result

$$\sin^2 \theta_W = 0.236 + 0.012(m_c - 1.5)$$
$$\pm 0.005(\text{exp.}) \pm 0.003(\text{theor.}), \qquad (11)$$

where m_c is the mass of the charm quark in GeV/c^2. The total theoretical uncertainty in the determination of $\sin^2 \theta_W$, excluding the uncertainty on m_c, is estimated to be of the order of ± 0.003.

Higher twist effects were neglected. To investigate their effects we repeated the analysis for hadron energies larger than 9 GeV; the values of $\sin^2 \theta_W$ are given in Table 12. In each case the 'raw' value is given, by simply substituting the measurements of R^ν and r in (10), and in addition the values after radiative corrections only and after radiative and quark-model corrections. The difference between the two values of $\sin^2 \theta_W$ is consistent with the statistical uncertainty of the event sample between 4 and 9 GeV hadron energy, combined with the different systematic errors from the hadron-energy threshold. The value of $\sin^2 \theta_W$ does not vary with the hadron-energy threshold, thus demonstrating the consistency of the methods used.

We can use the measurement of R^ν to investigate the consistency with the assumption of $\varrho = 1$. Figure 15 shows the quark-model prediction for R^ν and $R^{\bar\nu}$ for a range of values of $\sin^2 \theta_W$. The shaded area along the curve indicates the theoretical uncertainty. For $\sin^2 \theta_W = 0.236$, the value derived from R^ν and

Table 12. $\sin^2 \theta_W$ values as a function of the E_h threshold

E_h threshold	$\sin^2 \theta_W^{\text{raw}}$	$\sin^2 \theta_W^{\text{rad}}$	$\sin^2 \theta_W^{\text{rad}+\text{qpm}}$
4 GeV	0.2356	0.2252	0.2359 ± 0.0050
9 GeV	0.2409	0.2302	0.2383 ± 0.0052
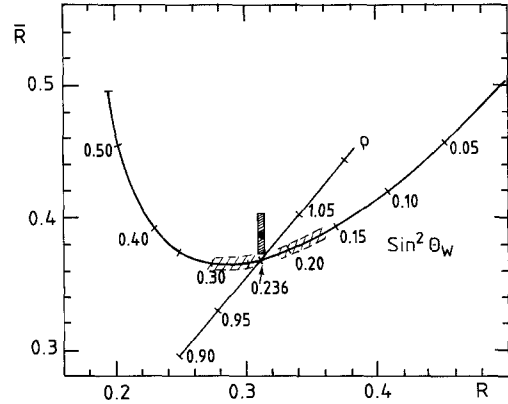
Fig. 15. Quark-model prediction for R^ν and $R^{\bar\nu}$ as a function of $\sin^2 \theta_W$ and ϱ

Table 13. Comparison of values of $\sin^2 \theta_W$ derived from semileptonic neutrino-scattering experiments. The common theoretical error is ±0.003

Group	Method	$\sin^2 \theta_W(\text{exp.})$
FMMF [29]	Event-by-event	0.246 ± 0.016
CCFR [31]	Event length	0.239 ± 0.010
CDHS [30]	Event length	0.225 ± 0.005
CHARM [32]	Event-by-event	0.236 ± 0.005

r, a range of ϱ values is indicated as well. We note good agreement with the model for $\varrho = 1.030 \pm 0.020$.

This result can be compared with those obtained in other semileptonic neutrino-scattering experiments. Starting from a previous measurement (1981) of R^ν and r by this Collaboration [7], and applying the same quark-parton model and radiative corrections, we obtained $\sin^2 \theta_W = 0.223 \pm 0.014(\text{exp.})$ (see Table 1). Our new result is compared with those obtained in other recent semileptonic neutrino-scattering experiments (see Table 13) for $m_c = 1.5$ GeV/c^2. The FMMF Collaboration at FNAL used a method similar to ours, classifying NC and CC interactions on an event-by-event basis [29]. The CDHS Collaboration at CERN [30] and the CCFR Collaboration at FNAL [31] used a statistical method for classification based on the total event length. The agreement is good and significant considering the differences in experimental procedures used. The mean value derived from these experiment is

$$\sin^2 \theta_W^{\text{average}} = 0.233 \pm 0.004(\text{exp.}) \pm 0.005(\text{theor.}). \qquad (12)$$

6 Discussion and conclusions

Using the new precise value of $\sin^2 \theta_W$ together with the recent direct measurements of m_W and m_Z [9, 10] we have determined the electroweak radiative shift

of the W mass from (6) and find

$$\Delta r = 0.077 \pm 0.025 (\text{exp.}) \pm 0.038 (\text{syst.}), \qquad (13)$$

in good agreement with the calculated correction of $\Delta r = 0.0713 \pm 0.0013$ assuming $m_t = 45$ GeV and $m_H = 100$ GeV [1, 11]. The systematic error of Δr is the quadratic sum of the theoretical uncertainties in determining $\sin^2 \theta_W$ from semileptonic neutrino scattering and of the energy scale error entering into the W and Z^0 mass determinations. The agreement between theory and experiment is very good. The value of $\sin^2 \theta_W$ obtained from deep inelastic ν_μ scattering without electroweak radiative corrections differs from the uncorrected value obtained from m_W and m_Z (see Table 1) by $\Delta \sin^2 \theta_W = 0.027 \pm 0.011$, where experimental, systematic and theoretical errors are combined quadratically. This difference is significant at the 2.5 σ level and illustrates quite nicely the existence of and need for radiative corrections. Assuming, therefore, their validity a precise determination of the ϱ parameter can be obtained using the relation

$$\varrho^2 = R^\nu / R^{\text{calc}},$$

where R^{calc} is calculated with (10) using the weighted average of $\sin^2 \theta_W$ measurements by the UA 1 [9] and UA 2 [10] Collaborations working at CERN of $\sin^2 \theta_W = 0.226 \pm 0.008$ and R^ν is corrected for radiative and quark-parton model corrections. Propagating the errors quadratically we find

$$\varrho = 0.990 - 0.013 (m_c - 1.5) \pm 0.009 (\text{exp.}) \pm 0.003 (\text{theor.}) \qquad (14)$$

in good agreement with the minimal Standard Model (m_c is the mass of the charm quark in GeV/c^2).

New physics appendages to the Standard Model or a different input value for m_t would modify the prediction of (4) and (5). We can therefore use the good agreement with experiment as a constraint. For example, if m_t were 250 GeV/c^2 Δr would become zero, whereas $\sin^2 \theta_W$ hardly changes [33]. From the present experimental value of Δr, Marciano and Sirlin [33] find the constraint.

$$m_t \lesssim 180 \text{ GeV}. \qquad (15)$$

In the case of a heavy fourth-generation charged lepton L with massless neutrino companion the corresponding bound is [33]

$$m_L \lesssim 300 \text{ GeV}. \qquad (16)$$

Future high-precision experiments should determine m_W and m_Z to ± 0.1 GeV and ± 0.02 GeV, respectively and, combined with the result of a determi-

nation of $\sin^2 \theta_W$ from $\nu_\mu e$ and $\bar{\nu}_\mu e$ scattering in the CHARM II experiment to ± 0.005 without theoretical uncertainty, should thus provide even better constraints or perhaps a hint of new physics.

Our final comment is concerned with the comparison of $\sin^2 \theta_W$ predicted by Grand Unified Theories. The experimental result presented here contradicts the prediction of the minimal $SU(5)$ model [1, 34],

$$\sin^2 \theta_W = 0.214 \pm 0.004 \quad [SU(5)], \qquad (17).$$

which has already been ruled out by the experimental lower limit of proton decay [35]. Equation (16) can be used to constrain the additional mass scales of non-minimal Grand Unified Theories. For example, in the case of supersymmetric theories (SUSY), the experimental result is in good agreement with the mass constraint $M_{\text{SUSY}} \gtrsim 1$ TeV [33].

References

1. For a recent review see, for example, U. Amaldi et al.: preprint CERN-EP/87-93, to be published in Phys. Rev. D
2. M.A. Bouchiat, C.A. Piketty: J. Phys. (France) 46 (1985) 1897; S. Gilbert, N. Noecker, R. Watts, C. Wiemann: Phys. Rev. Lett. 55 (1985) 2680
3. C.Y. Prescott et al.: Phys. Lett. 77B (1978) 347, 84B (1979) 524
4. CHARM Collab. F. Bergsma et al.: Phys. Lett. 147B (1984) 481
5. L.A. Ahrens et al.: Phys. Rev. Lett. 54 (1985) 18
6. K. Abe et al.: Phys. Rev. Lett. 56 (1986) 1107
7. CHARM Collab. M. Jonker et al.: Phys. Lett. 99B (1981) 265
8. CDHS Collab. H. Abramowicz et al.: Z. Phys. C – Particles and Fields 28 (1985) 51
9. UA 1 Collab. S. Geer: Proc. Int. Conf. on High Energy Physics, Berkeley, 1986, vol. 2, p. 982. Singapore: World Scientific 1987
10. UA 2 Collab. R. Ansari et al.: Phys. Lett. 190B (1987) 238
11. W.J. Marciano, A. Sirlin: Phys. Rev. D22 (1980) 2695; Erratum Phys. Rev. D31 (1985) 213; Nucl. Phys. B189 (1981) 442; J.F. Weather, C.H. Llewellyn Smith: Nucl. Phys. 208 (1982) 27; Erratum Nucl. Phys. B226 (1983) 547
12. C.H. Llewellyn-Smith: Nucl. Phys. B228 (1983) 205
13. See, for example, a recent review by M. Diemoz, F. Ferroni, E. Longo: Phys. Rep. 130 (1986) 293
14. A. Grant, J.M. Maugain: Internal Report CERN/EF/BEAM 83-2
15. J. Panman: Contribution to Workshop on SPS Fixed-Target Physics in the years 1984–1989, CERN 83-02, p. 80. (1980)

16. CHARM Collab. A.N. Diddens et al.: Nucl. Instrum. Methods 178 (1980) 27; C. Bosio et al.: Nucl. Instrum. Methods 157 (1978) 35; CHARM Collab. M. Jonker et al.: Nucl. Instrum. Methods 200 (1982) 183

17. CHARM Collab. J. Dorenbosch et al.: Nucl. Instrum. Methods A 253 (1987) 203

18. CHARM Collab. M. Jonker et al.: Phys. Lett. 107B (1981) 241

19. R.M. Barnett: Phys. Rev. D 14 (1976) 70; H. Georgi, H.D. Politzer: Phys. Rev. D 14 (1976) 1829

20. D.Yu. Bardin, O.M. Dokuchaeva: preprint JINR-E2-86-260 (1986); D.Yu. Bardin, O.M. Federenko: Yad. Phys. 30 (1979) 811 [Transl. Sov. J. Nucl. Phys. 30 (1979) 418]; D.Yu. Bardin, O.M. Dokuchaeva: Yad. Phys. 36 (1982) 482 [Transl. Sov. J. Nucl. Phys. 36 (1982) 282]

21. A. Sirlin: Phys. Rev. D 22 (1980) 971

22. R.G. Stuart: Z. Phys. C – Particles and Fields 34 (1987) 445

23. V. Barger, R.J.N. Phillips: Nucl. Phys. B 73 (1974) 269

24. I. Liede, E.A. Paschos, M. Roos, S. Sakakibara: Helsinki University preprint HU-TFT-83-45; I. Liede, M. Roos, S. Sakakibara: Helsinki University preprint, HU-TFT-84-28

25. CDHS Collab. J. Knobloch et al.: Private communication

26. CDHS Collab. H. Abramowicz et al.: Z. Phys. C – Particles and Fields 17 (1983) 283

27. EMC Collab. J.J. Aubert et al.: Nucl. Phys. B 213 (1983) 31

28. K. Kleinknecht, B. Renk: Phys. Lett. 130B (1983) 459

29. FMMF Collab. D. Bogert et al.: Phys. Rev. Lett. 55 (1985) 1969

30. CDHS Collab. H. Abramowicz et al.: Phys. Rev. Lett. 57 (1986) 298

31. CCFRR Collab. P. Reutens et al.: Phys. Lett. 152B (1985) 404

32. CHARM Collab. J.V. Allaby et al.: Phys. Lett. 177B (1986) 446

33. W.J. Marciano, A. Sirlin (to be published); W.J. Marciano: Proc. 23rd Int. Conf. on High Energy Physics, Berkeley, 1986, vol. 2, p. 999. Singapore: World Scientific 1987; W.J. Marciano, A. Sirlin: Phys. Rev. D 29 (1984) 945; Erratum Phys. Rev. D 31 (1985) 213

34. W.J. Marciano, A. Sirlin: Phys. Rev. Lett. 46 (1981) 163

35. M. Goldhaber: Proc 23rd Int. Conf. on High Energy Physics, Berkeley, 1986, vol. 1, p. 248. Singapore: World Scientific 1987